Chin. J. Mech. Eng. (2017) 30:321–331
DOI 10.1007/s10033-017-0086-4

ORIGINAL ARTICLE

Work Hardening Behavior of 1020 Steel During Cold-Beating Simulation

Fengkui CUI[1,2] · Yuanfei LING[1,2] · Jinxue XUE[1,2] · Jia LIU[1,2] · Yuhui LIU[1,2] · Yan LI[3]

Received: 17 November 2016 / Revised: 28 December 2016 / Accepted: 6 January 2017 / Published online: 17 March 2017

Abstract The present research of cold-beating formation mainly focused on roller design and manufacture, kinematics, constitutive relation, metal flow law, thermo-mechanical coupling, surface micro-topography and microstructure evolution. However, the research on surface quality and performance of workpieces in the process of cold-beating is rare. Cold-beating simulation experiment of 1020 steel is conducted at room temperature and strain rates ranging from 2000 to 4000 s^{-1} base on the law of plastic forming. According to the experimental data, the model of strain hardening of 1020 steel is established, Scanning Electron Microscopy(SEM) is conducted, the mechanism of the work hardening of 1020 steel is clarified by analyzing microstructure variation of 1020 steel. It is found that the strain rate hardening effect of 1020 steel is stronger than the softening effect induced by increasing temperatures, the process of simulation cold-beating cause the grain shape of 1020 steel significant change and microstructure elongate significantly to form a fibrous tissue parallel to the direction of deformation, the higher strain rate, the more obvious grain refinement and the more hardening effect. Additionally, the change law of the work hardening rate is investigated, the relationship between dislocation density and strain, the relationship between work hardening rate and dislocation density is obtained. Results show that the change trend of the work hardening rate of 1020 steel is divided into two stages, the work hardening rate decreases dramatically in the first stage and slowly decreases in the second stage, finally tending toward zero. Dislocation density increases with increasing strain and strain rate, work hardening rate decreases with increasing dislocation density. The research results provide the basis for solving the problem of improving the surface quality and performance of workpieces under cold-beating formation of 1020 steel.

Keywords 1020 steel · Cold-beating · Work hardening · Grain · Dislocation density

1 Introduction

The high-quality carbon structural steel known as 1020 steel is widely-used in gears, splines, ball screw and many other parts due to the good plasticity and toughness exhibited by materials formed by cold-beating. The technology of high-speed cold-beating forming applies the characteristic of the plastic forming of mental and uses the high-speed beating roller to roll and beat the blank so that it is an environmental and near-net forming processing method of making mental flow into parts profile [1]. However, the forming process is accompanied by the work hardening of a workpiece surface due to mechanical force. Work hardening is one of the important indexes for evaluating the surface quality of workpiece, it is also one of the important factors that affect the surface integrity. Work

Supported by National Natural Science Foundation of China (Grant Nos. 551475146, 51475366, 51075124).

✉ Yuanfei LING
18937976427@163.com

[1] School of Mechatronics Engineering, Henan University of Science and Technology, Luoyang 471003, China

[2] Collaborative Innovation Center of Machinery Equipment Advanced Manufacturing of Henan Province, Henan University of Science and Technology, Luoyang 471003, China

[3] School of Mechanical and Precision Instrument Engineering, Xi'an University of Technology, Xi'an 710048, China

hardening can improve the hardness and wear resistance of the workpiece, improve the yield limit of the material and enhance its resistance to deformation, but the wear of the rolling wheel is simultaneously increased. In order to improve the surface quality and performance of a cold-beating formation workpiece and prolong the service life of rolling wheels, the cold-beating formation mechanism of 1020 steel was analyzed, and a model of work hardening was established. This work is of great theoretical significance and of value to many engineering applications.

In the past ten years, extensive studies have been carried out on cold-beating forming technology, which is represented by the research group in Xi'an University of Technology and Henan University of Science and Technology. In the design and manufacture of rollers, CUI, et al. [2–4], used forming method to design and manufacture rollers without inaccurate outline, and built up a math model of rollers outline design, in which the experimental method was applied to correct the theoretical outline of rollers. They developed a simulation system of rollers, verified the correctness of the design and manufacture of rollers and carried out a series of process experiments of actual spline shaft, which made the formation of cold-beating have higher machining precision. From the aspect of kinematics, MA, et al. [5], analyzed the theory of interference phenomenon between cold-beating and workpieces, designed and improved the structure of cold-beating head. Without changing the rollers' outline, the forming error was reduced and the reasonability of the improvement of cold-beating head's structure was also tested with experiments. LI, et al. [6], applied the software Deform to analyze this technology at various deformation areas, in various temperature, at various rate, which made the foundation of deeply studying the technology of high-speed cold-beating forming. Using the method of simulation and experiments, YUAN, et al. [7], analyzed the deformation force and effect law between the technological parameter and deformation force during the process of cold-beating forming of block materials, the results of which provide effective evidence of the choice of technological parameter and the control of the forming process. In the constitutive relation, LI, et al. [8, 9], carried out the SHPB experiments of 40Cr under various kinds of temperatures and rates and built up a constitutive model of dynamic plasticity of cold-beating. They also made a comparison between the stress–strain relationship predicted by the model and the experiment status, which tested the correctness of the model and indicated the relationship between the macroscopical deformation and formability effect and thus provided theoretical base for studying the process of cold-beating. In the metal flow, QUAN, et al. [10, 11], built up a local contact model of rollers and spline shaft base during the cold round-beating forming process. According to the metal law of least resistance, the flow of metal in the cold-beating forming area was analyzed and the simulation value was gathered to get the motion trail of forming area node. Besides, they also discussed the forming node coordinate variation trend of single pass cold-beating and summarized the metal flow rule during the process of cold-beating. In the regard of thermo-mechanical coupling forming theory, ZHANG, et al. [12, 13], conducted the analysis of theoretical model based on thermo-mechanical coupling, which showed that the heat dissipation of irreversible plastic and the effect of the generation of heat by friction on the workpiece and the section of beating roll caused the production of heat during the cold-beating forming. In addition, the center point of fields coupling is the energy transformation during the process of cold-beating forming. In the surface micro-topography, LIANG, et al. [14], analyzed the reasons of the ripple that formed during the cold-beating process and then found out the expression of the ripple's height, which was corrected according to simulation results. Besides, the ripple which was produced on the workpiece's surface during the cold-beating process was measured and compared between the theory and experiments, which tested the correctness of the expression of ripple's height after correction. From the aspect of microstructure evolution, WANG, et al. [15, 16], have built up evolution models of microstructure, which is based on dislocation density of 40Cr. The study has identified the connection between the macroscopic and microcosmic of cold-beating forming, and explained the change law of 40Cr during the process of cold-beating forming.

Many scholars conducted research focused on the work hardening behavior of materials by combining theoretical and experimental analyses. RENARD, et al. [17], reported the changes in the work hardening rate and microstructure of TWIP steel revealed by tensile test at high temperatures; the relationship between the work hardening and twinning rates of TWIP steel was analyzed, a method for predicting the twinning rate of TWIP steel was proposed, and the reliability of the proposed method was verified by an Electron Backscatter Diffraction experiment. YANG, et al. [18], established a mathematical model describing the relationship between the work hardening rate and the stress/strain of titanium alloys. The work hardening effect is characterized by obvious stages as strain is applied: steady fluctuations with a linear decrease. The work hardening effect of titanium alloys is obvious at low temperature and high strain rates; the work hardening rate increases rapidly with increases in temperature, while the strain rate simultaneously decreases. WANG, et al. [19], established the dynamic recrystallization model of low carbon steel based on data obtained from compression tests at high temperatures and low strain rates; the critical conditions of the dynamic recrystallization of low carbon

steel were determined based on the strain hardening curve. The work hardening and dynamic softening mechanisms of low carbon steel in a hot forming process were also analyzed; results indicate that higher volume fractions of dynamic recrystallization result in Z values (model parameter). BUI, et al. [20], compared the finite element simulation and experimental results of the cold roll-forming process applied to steel sheet; results indicate that the quality of the steel sheet manufactured by cold roll-forming is primarily influenced by the yield limit and the exponent of work hardening, and that formation speed and fiction coefficient provide minor influence. This conclusion provides the basis for the optimization of the cold roll-forming process.

SARKAR, et al. [21], established a work hardening model of an α-Ti alloy based on tensile test data after the materials were aged at different temperatures; the work hardening characteristics of a α-Ti alloy were reported from a microscopic perspective, based on transmission electron microscopy. SINCLAIR, et al. [22], studied the work hardening behavior of polycrystalline copper based on tensile tests conducted at low temperatures; results indicate that during the initial plastic deformation stage, grains size has a dominant effect on the work hardening of polycrystalline copper. When the strain is large, grain size has no effect on work hardening due to the dynamic recovery effect of the grain boundary. DEL VALLE, et al. [23], studied magnesium-based alloys formed with various plastic deformation methods(equal channel angular pressing and large-strain hot rolling); results indicate that the changing basal slip orientation factor effects both dislocation storage and dynamic recovery, and that refinement of the grain size induces a strong decrease in the work hardening rate. A reasonable explanation for these phenomena is provided by the grain boundary sliding theory. DAS, et al. [24], analyzed the microstructure of low carbon ferrite-martensite dual-phase steel affected by different heat treatments by using the Crussard-Jaoul method, which consists of three work hardening stages which enable intermediate quenching and intercritical annealing samples, whereas the step quenching samples were exposed to only two stages. The work hardening behavior observed with intermediate quenching leads to the current analysis of low-carbon ferrite-martensite dual-phase steel with high strength and good ductility as influenced by different methods of heat treatment.

The present research of cold-beating formation is mainly focus on roller design and manufacture, kinematics, constitutive relation, metal flow law, thermo-mechanical coupling, surface micro-topography and microstructure evolution, and the study on work hardening of 1020 steel mainly include quenching and quenching plus tempering treatments [25], fine-blanking with negative clearance [26], laser transformation [27], plasma-electrolysis boronizing [28]; however, there is no report to date regarding the work hardening of 1020 steel formed by cold-beating. Therefore, in this paper, the model of strain hardening of 1020 steel was established based on simulation cold-beating data, the microscopic mechanism of 1020 steel was verified by SEM and the relationship among the three of work hardening rate, strain and dislocation; the aim of the current work is to improve the surface quality and performance of 1020 steel under cold-beating by controlling work hardening degree.

2 Cold-Beating Simulation Experiment

2.1 Experiment Materials

The experiment used 1020 steel; the chemical composition of 1020 steel is depicted in Table 1. All studied specimens were cylindrical with a diameter of Φ8 mm and a length of 6 mm, and the hardness value equal to 160–170 HB. The specimen fabrication procedure consisted of turning, wire cutting and grinding.

2.2 Experiment Equipment

Dynamic characteristic tests were conducted at various strain rates using a cold-beating simulation apparatus, as shown in Fig. 1. The microstructure of specimens was observed using a JSM-5610LV scanning electron microscope apparatus, as shown in Fig. 2.

2.3 Experiment Parameters

The specimens were divided into four groups; each group was tested at a strain rate of 2000 s^{-1}, 2500 s^{-1}, 3000 s^{-1} and 4000 s^{-1}. The experiments were all conducted at room temperature.

2.4 Experiment Procedures

Device schematic of Simulation of cold-beating apparatus is shown in Fig. 3. Two ends of the specimens were smeared with polishing paste (Al_2O_3), and were polished with a polishing machine until all obvious surface scratchers were eliminated. The cold-beating experimental simulation was conducted at various strain rates. The polished surface of each specimen was wiped with alcohol,

Table 1 Chemical composition of 1020 steel (mass fraction, %)

C	Si	Mn	P	S	Ni	Cr
0.20	0.17–0.37	0.35 ~ 0.65	≤0.035	≤0.035	≤0.30	≤0.25

Fig. 1 Simulation of cold-beating apparatus

Fig. 2 JSM-5610LV scanning electron microscope apparatus

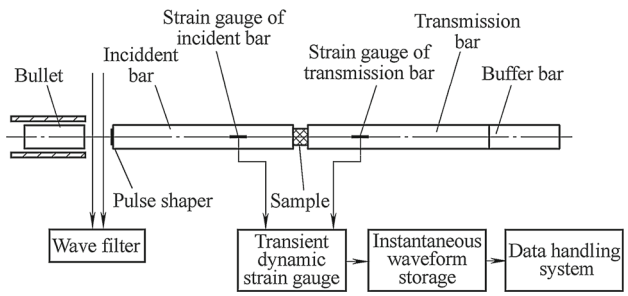

Fig. 3 Device schematic of Simulation of cold-beating apparatus

after which the surfaces of all specimens were smeared with lithium-based grease to reduce the effect of friction on the end face. Changes in strain rate were achieved by adjusting the pressure of the high pressure chamber in the transmitting device to control the velocity of the bullet. The gas chamber pressure of the four respective groups was 0.4 MPa, 0.5 MPa, 0.7 MPa, 0.9 MPa. The velocity of the bullet impact specimen was measured by a laser measurement device. The contact surface between the specimen and the impact rod was machined until it was smooth to ensure that the surfaces could achieve full contact. The two strain gauges were connected in series and pasted onto the impact bar. Experimental data was extracted from the recorded intelligent measurements; the incident wave, reflected wave and transmitted wave were obtained from the strain indicator based on the measurement system of the experiment table.

The surface of specimens under cold-beating formation simulation were cleaned with acetone before being corroded by an alcohol solution containing 3% nitrate until the surface was gray, and corrosion ceased to progress. Next, the surfaces of all specimens were dried after washing with distilled water; a high vacuum was initialized after the specimens were placed on the instrument table. When the appropriate vacuum degree was reached, the electron gun automatically increased the pressure 20 kv, and the scanning electron microscope entered the working state. Satisfactory images were obtained by moving the sample table near the computer, adjusting the magnification and focus, and observing the specimens' surfaces. Still photos were taken of the surface microstructures. The specimens were then cut along the axis by a wire cutting machine, and the half-cylindrical specimens were embedded. After being finished, the side faces of all specimens were polished and corroded, and the microstructure of the layer depth direction was observed by scanning electron microscope.

2.5 Experiment Results

The relationship between the stress, strain and strain rate of the materials with respect to time were obtained based on 1D stress wave theory [29]. Engineering stress and strain were transformed into true stress and strain, and the average values of the four experimental groups were respectively obtained:

$$\sigma_E = E\frac{A_\mathrm{b}}{A_\mathrm{s}}\varepsilon_\mathrm{T}R, \tag{1}$$

$$\varepsilon_E = \frac{2C_0}{L}\int_0^t \varepsilon_R \mathrm{d}t, \tag{2}$$

$$\dot{\varepsilon}_E = \frac{2C_0}{L}\varepsilon_R, \tag{3}$$

where A_b represents cross section area of compression bar, As represents cross section area of sample, ε_T represents transmission wave pulse, ε_R represents reflected wave pulse, L represents the length of sample, C_0 represents elastic wave velocity of compression bar, $C_0 = \sqrt{E/\rho}$, E represents elastic modulus of sample, ρ represents density of sample.

The true stress–strain curve of 1020 steel at different strain rates is shown in Fig. 4. Figure 5 depicts the original microstructure of a 1020 steel specimen. The surface microscope of 1020 steel specimens exposed to cold-beating at different strain rates is shown in Fig. 6. The microstructure of the side face of 1020 steel specimens undergoing cold-beating simulation at different strain rates is shown in Fig. 7.

3 Work Hardening Mechanism of 1020 Steel

It is known that the cold-beating process includes an elastic deformation stage and a plastic deformation stage, as shown in Fig. 4. The plastic deformation of 1020 steel at a high strain rate is a competitive process of the strain hardening effect, strain rate hardening effect and the softening effect induced by rising temperatures. During the plastic deformation stage, the true stress of 1020 steel increased with increasing strain and strain rate, indicating that the strain rate hardening effect of 1020 steel is stronger than the softening effect induced by increasing temperatures.

According to Fig. 5, the original microstructure of 1020 steel is ferrite and pearlite, ferrite; pearlite grains are distributed in the shape of a cell, the grain boundary is obvious, pearlite is randomly arranged in various directions, and the microstructure consists of a present sheet layer shape with relatively uniform distribution. According to Fig. 6, the lattice was broken during the plastic deformation process of the cold-beating simulation; although pearlite was observed in a sheet layer shape, several fragments of the pearlite interior formed a large number of interfaces which divided the ferrite into fine grains and resulting in non-identical atoms in different grains. The pearlite stripe was no longer uni-directional, and the ferrite grains became more refined as strain and strain rate increased. According to Fig. 7, the equiaxed ferrite grains in the direction of layer depth were twisted and bent, which

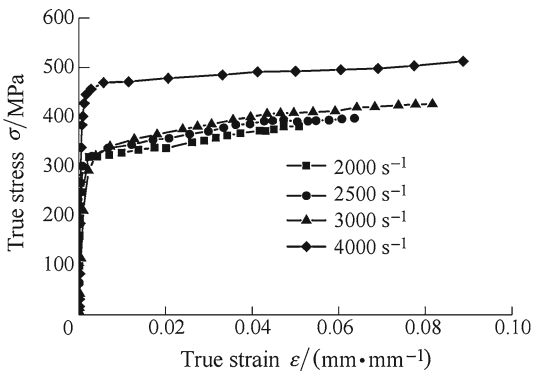

Fig. 4 True stress–strain curve of 1020 steel at different strain rates

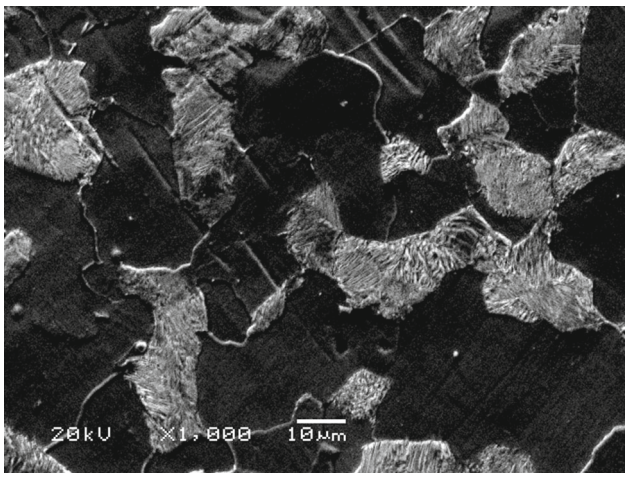

Fig. 5 Original microstructure of 1020 steel

appeared to follow a certain direction and gradually extended to the direction of deformation; fine and larger pearlite grains were distributed and criss-crossed along the ferrite boundaries. As strain accumulated, the pearlite pellet became ambiguous, the sheet layer space was reduced, the degree of bending and torsion became increasingly extreme, and the microstructure elongated significantly to form a fibrous tissue parallel to the direction of deformation. Grain refinement created increasing grain boundaries which hindered the slip of dislocation; thus, the dislocation was stored and dislocation density increased, which in turn enhance resistance to material deformation and improve fatigue life [30].

The macro-performance perspective reveals the work hardening effect. The short duration of the cold-beating simulation indicates that the process may be considered to be an adiabatic temperature rise, in which heat generated by plastic deformation increased the free energy of the material. Material in a metastable state has a tendency to transform prior to deformation, increasing the motion of dislocation; the intersection between positive and negative would lead to dislocation annihilation, so as to decrease the dislocation density. The dislocation slip was easily observed, verifying that the macro-performance demonstrated a dynamic softening effect.

4 Establishment of Strain Hardening Model of 1020 Steel

The strain hardening law proposed by Voce [31], which describes the variation of stress values from initiation to saturation at a given strain rate and temperature, it can be expressed as follows:

$$\sigma = \sigma_S - (\sigma_S - \sigma_I)\exp[n_V(\varepsilon - \varepsilon_I)], \quad (4)$$

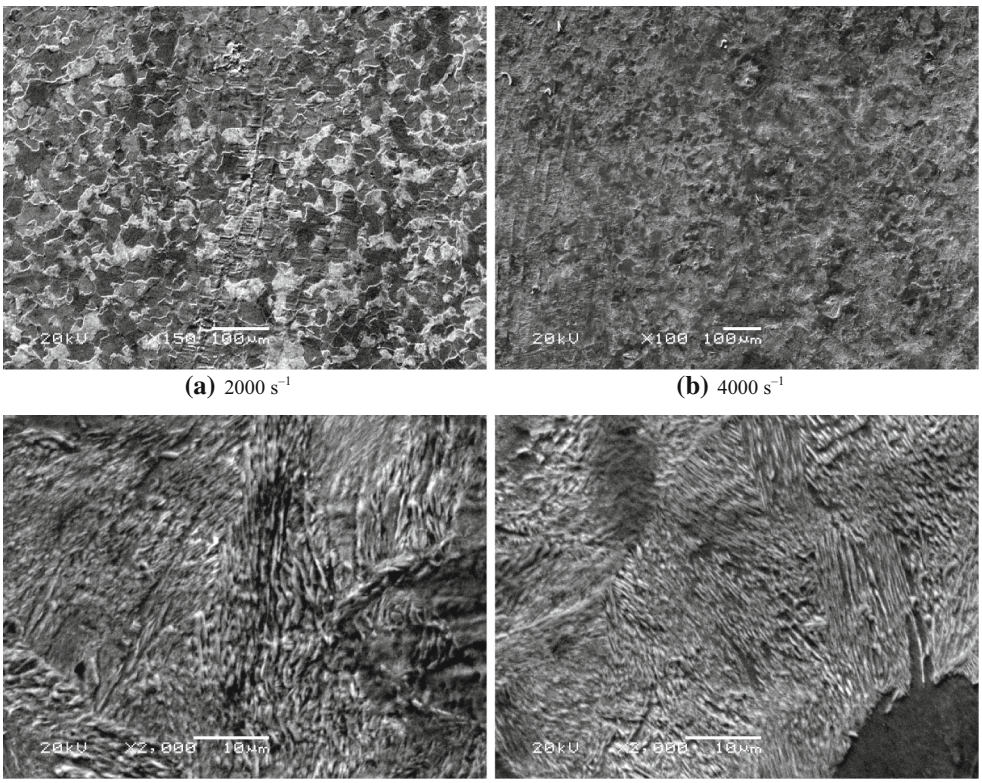

(a) 2000 s^{-1} **(b)** 4000 s^{-1}

(c) 2000 s^{-1} **(d)** 4000 s^{-1}

Fig. 6 Microstructure of the side face of specimens at different strain rates

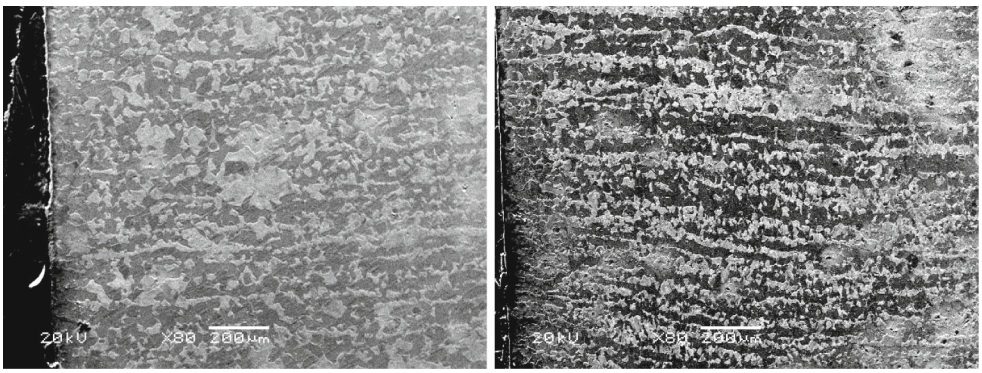

(a) 2000 s^{-1} **(b)** 4000 s^{-1}

Fig. 7 Microstructure of the side face of specimens at different strain rates

where σ_S represents the saturation stress; σ_I and ε_I represent true stress and true stain at the onset of plastic deformation, respectively; and n_V is a material parameter. Least squares was done between Voce model and experimental data representing plastic deformation at different strain rates, as shown in Fig. 8.

It is known that flow stress at different strain rates predicted by the Voce model are consistent with the experimental data depicted in Fig. 8, indicating that the Voce model can accurately reflect the real experimental situation and effectively predict the flow stress of 1020 steel at different strain rates. The Voce model parameters are shown in Table 2.

5 Change Law of work Hardening Rate of 1020 Steel

The work hardening rate refers to the degree of speed variation of flow stress of a material with increasing strain during the process of plastic deformation. The work

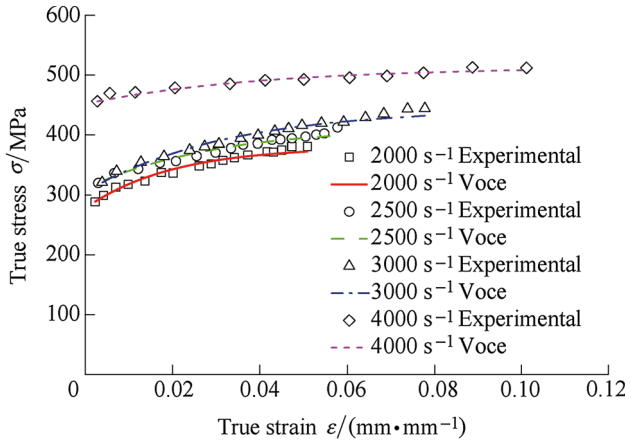

Fig. 8 Experimental data at different strain rates fixed by the Voce model

Table 2 Voce model parameters at different strain rates

Strain rate $\dot{\varepsilon}$/s^{-1}	2000	2500	3000	4000
Initial stress σ/MPa	288.8	320.4	340.1	445.1
Saturation stress σ/MPa	381	412.5	444.5	512.8
Initial strain ε/(mm·mm^{-1})	0.002 3	0.003 0	0.007 0	0.001 6
Parameter n_v	–50	–35	–27	–25

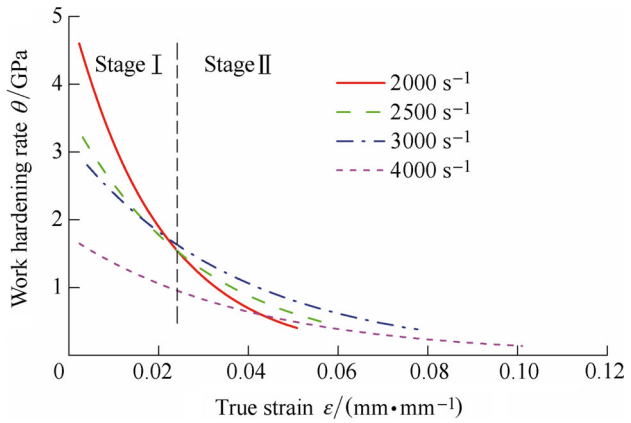

Fig. 9 Relationship between work hardening rate and true strain at different strain rates

hardening rate is derived according to the following definition [32]:

$$\theta = \frac{\mathrm{d}\sigma}{\mathrm{d}\varepsilon}. \tag{5}$$

The relationship between the work hardening rate and the strain curves of 1020 steel under different strain rates shown in Fig. 9, derived according to Eq. (5) and the parameters detailed in Table 2. The trend in the work hardening rate of 1020 steel at different strain rates is nearly identical, and divided into two primary stages. In the first stage, the work hardening rate is greater at the onset of plastic deformation, and decreases dramatically as strain increases. In the second stage, the work hardening rate slowly decreases as strain increases, finally tending toward zero. In the first stage, the lower strain rate and lower work hardening rate is directly contrary to those observed during the second stage, indicating that 1020 steel strengthened as strain rate increased during the first stage and weakened as strain increased during the second stage. The deformation of 1020 steel is primarily induced by ferrite after the yield limit is reached, when the deformation of ferrite grains are restrained by the surrounding grains due to polycrystalline continuity, which simultaneously creates numerous slip systems in the vicinity of the grain boundary [33]. The deformation of ferrite grains can produce a large number of dislocations distributed in the vicinity of the pearlite, in which the resistance to dislocation slip is very high.

Under high strain rates, the average velocity of dislocation motion increases as strain rate increases. Many dislocations were quickly hindered in the vicinity of grain boundaries, which formed a collection of dislocations and led the dislocation density to increase dramatically, subsequently increasing the work hardening rate of the 1020 steel. The work hardening rate decreased rapidly as strain increased because the accumulation of dislocations on the same slip plane formed a barrier at the front; the back of the dislocation on the main slip crossed the barrier and continued to move forward, inducing the increase in stress speed as strain increased.

The heat generated by the plastic deformation increased with increasing strain, which caused temperature rise near the ferrite-pearlite grain boundaries; the pearlite was more prone to deformation, thus weakening the strain hardening effect of ferrite, and making dislocation slip more easily achievable. The hardening effect was offset by the softening effect induced by rising temperatures; the temperature-related softening effect became gradually more pronounced, eventually becoming dominant. This caused the strain to increase to a certain threshold value, at which the work hardening rate decreased slowly as strain continued to increase. At this time, as strain increased, the strain hardening effect entered into the second progressive stage, in which hardening ferrite and pearlite were deformed, and the refinement of ferrite improved the plastic deformation barrier. Higher strain rates resulted in more dramatic ferrite refinement, explaining why the strain hardening effect of 1020 steel entered into the second stage as strain rate continued to increase. As shown in Fig. 8, obvious reflection points resulted from the stacking fault energy of 1020 steel. The dislocation slip and climb was more prone to occur [34], forcing the plastic deformation of 1020 steel into the second stage, corresponding with small strain values.

6 Micro Model of Work Hardening of 1020 Steel

The dislocation is distributed uniformly on the surface of each specimen; each dislocation segment is divided into locking dislocation and mobile dislocation. The flow stress is primarily affected by mobile dislocation, which is approximately equal to the total dislocation density of the specimen. The Taylor relation [35] has been widely-used to characterize the flow stress response to dislocation density in plastic deformation:

$$\sigma = M\alpha Gb\sqrt{\rho}, \tag{6}$$

where M represents the average Taylor factor ~ 3.06, α represents the Taylor constant ~ 0.5, G represents the shear modulus $\sim 1.7 \times 10^5$ MPa, and b represents the Burgers vector $\sim 3.2 \times 10^{-8}$ cm. The strain hardening and dynamic softening effects on dislocation density can further influence flow stress. Strain hardening leads to increasing dislocation density; dynamic softening leads to decreasing dislocation density. During the cold-beating simulation process, the change in dislocation density with increasing strain is determined by two segments [36]:

$$\mathrm{d}\sigma/\mathrm{d}\varepsilon = \mathrm{d}\rho/\mathrm{d}\varepsilon\big|_{\text{storage}} - \mathrm{d}\rho/\mathrm{d}\varepsilon\big|_{\text{recovery}}. \tag{7}$$

Kocks proposed that the square root of the dislocation density of a material is proportional to the increasing speed of dislocation density, and that the decrease in dislocation density is related to the absolute value of dislocation density. Based on findings of previous studies, the KOCKS model [37] is widely-used to describe the relationship between the dislocation density of a material and strain in plastic deformation. During the plastic deformation stage of 1020 steel, stress value does not fluctuate and dislocation density changes obviously with the increase of strain under the same stain rate, Kocks model can be used to show the change of dislocation density of 1020 steel shown in the following equation:

$$\frac{\mathrm{d}\rho}{\mathrm{d}\varepsilon} = k_1\sqrt{\rho} - k_2\rho, \tag{8}$$

where k_1 represents the hardening coefficient, k_2 represents softening coefficient, and $k_2 = -2n_v$.

Eq. (8) can be expressed by the following integral:

$$\sqrt{\rho} = \frac{k_1}{k_2} + \left(\sqrt{\rho_0} - \frac{k_1}{k_2}\right)\exp\left(-\frac{k_2}{2}(\varepsilon - \varepsilon_0)\right). \tag{9}$$

The dislocation storage and annihilation reached a balanced state when the stress value reached its peak, and the work hardening rate $\theta = 0$. Eq. (8) can be expressed as follows:

$$\sqrt{\rho_s} = \frac{k_1}{k_2}. \tag{10}$$

Eq. (6) can be expressed as follows:

$$\sqrt{\rho_s} = \frac{\sigma_s}{M\alpha G_b}. \tag{11}$$

The value of k_1, k_2 at different strain rates were obtained according to the experimental data as shown in Fig. 2, Eqs. (8), (10) and (11), and are summarized in Table 3.

The following equation can be obtained according to Eqs. (9) and (10):

$$\rho = \left[\sqrt{\rho_s} - \left(\sqrt{\rho_s} - \sqrt{\rho_0}\right)\mathrm{e}^{\frac{k_2}{2}(\varepsilon-\varepsilon_0)}\right]^2. \tag{12}$$

The relationship between the dislocation density and strain at different strain rates was obtained according to Eq. (12), the parameters from Table 3, and experimental data from Fig. 2. As shown in Fig. 10, the dislocation density is relatively large when the strain rate is equal to 4000 s^{-1}, the dislocation density is relatively small when the strain rate is equal to 2000 s^{-1}, and dislocation density increases with increasing strain rate. The primary explanation for this is that as strain increases, the deformation is completed in a shorter amount of time; the number of dislocations, the velocity of the dislocation motion and the opportunity of dislocation intersect increased, which led flow stress accelerate significantly. The strain hardening of 1020 steel caused by dislocation density increased with increasing strain, which induced the curve to rise under high strain rates; alternatively, the dynamic softening effect of 1020 steel caused by the heat generated by fast plastic deformation decreased dislocation density rapidly, inducing the curve to rise and tend to a constant under high strain rates.

There are two main factors that affect the hardening rate during plastic deformation: one is the internal factor, that is, the characteristics of the material itself such as shear modulus, Burgers vector, etc.; the other is the external factor, that is, strain, strain rate and temperature, affect the hardening rate by affecting the dislocation density.

$$\theta = \frac{\mathrm{d}\sigma}{\mathrm{d}\varepsilon} = \frac{\mathrm{d}\sigma}{\mathrm{d}\rho}\cdot\frac{\mathrm{d}\rho}{\mathrm{d}\varepsilon} = \frac{M\alpha G_b}{2\sqrt{\rho}}\left(k_1\sqrt{\rho} - k_2\rho\right). \tag{13}$$

The relationship between the work hardening rate and dislocation density at different strain rates was obtained according to the parameters from Table 3 and results shown in Fig. 11. The initial and final dislocation density

Table 3 Parameter values at different strain rates

Strain rate $\dot{\varepsilon}$/s^{-1}	2000	2500	3000	4000
$k_1/10^6$	4.58	3.47	2.8	3.08
k_2	381	70	54	50

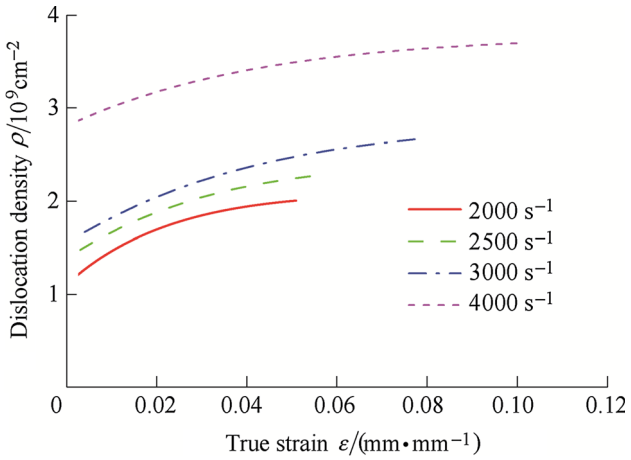

Fig. 10 Relationship between dislocation density and strain

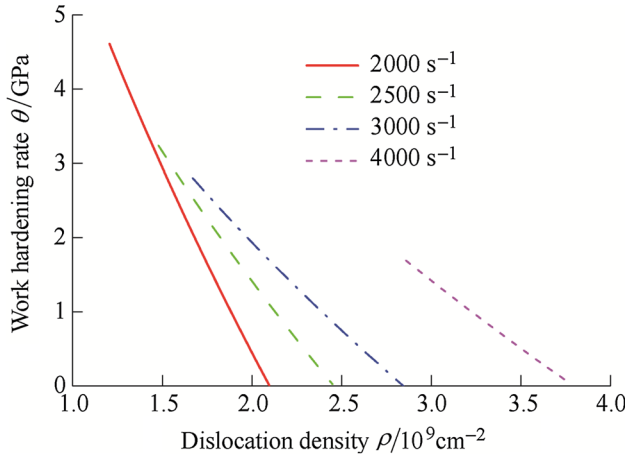

Fig. 11 Relationship between work hardening rate and dislocation density

of 1020 steel increased with increasing strain rate during plastic deformation; lower strain rates resulted in more obvious decreases in the work hardening rate and increases in dislocation density. The increasing strain rate accelerated the dislocation movement, leading the dislocation accumulation to be completed in a short amount of time, leading to greater dislocation of 1020 steel at the beginning of plastic deformation, especially at the strain rate of 4000 s^{-1}. As the stress exceeded the lattice friction, the dislocation near the lattice was rapidly released, and the dislocation density was offset due to the interaction of dislocation motion; the accumulation rate of dislocation decreased, thus decreasing the work hardening rate as strain rate increased. Higher strain rates resulted in slower decreases of the work hardening rate.

Hardening and softening occurred simultaneously during the simulation of high speed cold-beating. From the micro-perspective, the storage and annihilation of dislocation occurred simultaneously. As strain rate increased, the effect of the dislocation accumulation was more obvious, which hindered the dynamic recovery, prolonged dynamic recrystallization, and resulted in the obvious phenomenon of work hardening. Plastic deformation is divided into two parts: the primary portion is converted into heat to increase the temperature of the specimen, and the remainder is used to induce microstructural change [38]. High strain rates generate more heat in unit time, resulting in more obvious softening effects. However, the hardening effect was still dominant before equilibrium. With the increase of strain and strain rate, more dislocation accumulates, resulting in a higher final dislocation density.

7 Conclusions

(1) The basic mechanical parameters of 1020 steel were obtained based on cold-beating simulation experiment; the Voce model was established based on experimental data to accurately describe the strain hardening of 1020 steel.

(2) The cold-beating simulation is affected by the strain hardening effect, strain rate hardening effect and dynamic softening effect, the strain hardening effect and strain rate hardening effect is obvious in the process of simulation cold-beating of 1020 steel, grains become more refined as strain and strain rate increase.

(3) The change trend of the work hardening rate of 1020 steel is divided into two stages. The work hardening rate decreases sharply and the strain hardening effect is weakened with the increase of strain rate during the first stage; the work hardening rate decreases slowly and the strain hardening effect is strengthened with increasing strain rate in the second stage.

(4) The relationship between dislocation density and strain, and between work hardening rate and dislocation density were obtained, results indicate that dislocation density of 1020 steel increases with increasing strain and strain rate, the work hardening rate decreases with increasing dislocation density.

References

1. CUI F K. *Study on High-speed precise forming with cold roll-beating technique*[D]. Xi'an: Xi'an Institute of Technology, 2007.
2. CUI F K, LI Y, ZHOU Y W, et al. Roller Modeling for involute spline and its amendment[J]. *Journal of Nanjing University of Aeronautics & Astronautics*, 2005, 37(s1): 99–101. (in Chinese)
3. CUI F K, LI Y, ZHOU Y W, et al. CAD system of roller for involute spline and simulation of grinding process[J]. *Chinese*

Journal of Mechanical Engineering, 2005, 41(12): 210–215. (in Chinese)
4. YANG J X, CUI F K, WANG X Q, et al. Design theory and experimental amends of involute spline roller[J]. *China Mechanical Engineering*, 2008, 19(4): 419–422. (in Chinese)
5. MA Q, LI Y, YANG M S, et al. Structure improvement of roll-beating head for continuous indexing cold roll-beating machine[J]. *Acta Armamentarii*, 2015, 36(8): 1587–1593. (in Chinese)
6. LI Y X, LI Y, YANG M S, et al. Simulation analysis for high speed cold roll-beating forming process of 40Cr steel. *Mechanical Science and Technology for Aerospace Engineering*, 2016, 35(4): 595–600. (in Chinese)
7. YUAN Q L, LI Y, YANG M S, et al. Research on deforming force of slab cold roll-beating[J]. *China Mechanical Engineering*, 2014, 25(2): 251–256. (in Chinese)
8. LI Y X, LI Y, YANG M S, et al. Determination of 40Cr Johnson-Cook dynamic constitutive equation for cold roll-beating forming process[J]. *Chemical Engineering Transactions*, 2015, 46: 1159–1164.
9. CUI F K, XIE K G, XIE Y F, et al. Constitutive model of cold roll-beating of 40Cr[J]. *Materials Research Innovations*, 2015, 19: 284–287.
10. QUAN J H, CUI F K, YANG J X, et al. Numerical simulation of involute spline shaft's cold rolling forming based on ANSYS/LS-DYNA[J]. *China Mechanical Engineering*, 2008, 19(5): 419–427. (in Chinese)
11. CUI F K, WANG X Q, ZHANG F S, et al. Metal flowing of involute spline cold roll-beating forming[J]. *Chinese Journal of Mechanical Engineering*, 2013, 26(5): 1056–1062.
12. ZHANG F S, YAO H B, CUI F K, et al. Research on coupled thermo-mechanical numerical simulation of high speed cold rolling for 40Cr quenched and tempered steel[J]. *Materials for Mechanical Engineering*, 2014, 38(8): 101–107. (in Chinese)
13. LI Y, LI Y X, YANG M S, et al. Analyzing the thermal mechanical coupling of 40Cr cold roll-beating forming process based on the Johson-Cook dynamic constitutive equation[J]. *International Journal of Heat and Technology*, 2015, 33(3): 51–58.
14. LIANG X M, LI Y, YANG M S, et al. Analysis and modification on characterization parameter of surface scale-texture for cold roll-beating forming parts[J]. *Mechanical Science and Technology for Aerospace Engineering*, 2016, 35(4): 606–613. (in Chinese)
15. WANG X Q, CUI F K, YAN G P, et al. Study on dislocation density change during cold roll-beating of 40Cr[J]. *China Mechanical Engineering*, 2013, 24(16): 2248–2256. (in Chinese)
16. CUI F K, YAN G P, LIU H, et al. Study on microstructure evolution during the cold roll-beating of 40Cr[J]. *Applied mechanics and Materials*, 2014, 490–491: 256–261.
17. RENARD K, JACQUES P J. On the relationship between work hardening and twinning rate in TWIP steels[J]. *Materials Science and Engineering: A*, 2012, 542: 8–14.
18. YANG N, NING Y Q, LIANG H Q, et al. Work-hardening effect and strain-rate sensitivity behavior during hot deformation of Ti-5Al-5Mo-5 V-1Cr-1Fe alloy[J]. *Materials & Design*, 2015, 82: 84–90.
19. WANG M H, LI Y F, WANG W H, et al. Quantitative Analysis of Work Hardening and Dynamic Softening Behavior of low carbon Steel Based on the Flow Stress[J]. *Materials & Design*, 2013, 45: 384–392.
20. BUI Q V, Ponthot J P. Numerical simulation of cold roll-forming processes[J]. *Journal of Materials Processing Technology*, 2007, 202(1–3): 275–282.
21. SARKAR R, MUKHOPADHYAY A, Ghosal P, et al. Effect of aged microstructure on the strength and working hardening behavior of Ti-15 V-3Cr-3Sn-3Al Alloy[J]. *Metallurgical and Materials Transactions A*, 2015, 46(8): 3516–3527.
22. SINCLAIR C W, POOLE W J, BRECHET Y. A model for the grain size dependent work hardening of copper[J]. *Scripta Materialia*, 2006, 55(8): 739–742.
23. DEL VALLE J A, CARRENO F, RUANO O A. Influence of texture and grain size on work hardening and ductility in magnesium-based alloys processed by ECAP and rolling[J]. *Acta Materialia*, 2006, 54(16): 4247–4259.
24. DAS D, CHATTOPADHYAY P P. Influence of martensite morphology on the work-hardening behavior of high strength ferrite-martensite dual-phase steel[J]. *Journal of Materials Science*, 2009, 44(11): 2957–2965.
25. LIAN J, JIANG Z, LIU J. Theoretical model for the tensile work hardening behaviour of dual steel[J]. *Materials Science and Engineering: A*, 1991, 147(1): 55–65.
26. LI J H, FAN W F, ZHANG Z M. Study on Working hardening for AISI-1020 and AISI-1045 steel fine-blanking with negative clearance[J]. *Key Engineering Materials*, 2010, 431-432: 405–408.
27. SO S, KI H. Effect of specimen thickness on heat treatability in laser transformation hardening[J]. *International Journal of Heat and Mass Transfer*, 2013, 61(1): 266–276.
28. BEJER M A, HENRIQUEZ R. Surface hardening of steel by plasma-electrolysis boronizing[J]. *Materials & Design*, 2009, 30(5): 1726–1728.
29. KARIEM M A, BEYNON J H, RUAN D. Misalignment effect in the split Hopkinson pressure bar technique[J]. *International Journal of Impact Engineering*, 2012, 47: 60–70.
30. MIAO H, MEI Q, YUAN J Y, et al. Low cycle fatigue and strengthening mechanism of cold extruded large diameter internal thread of Q460 steel[J]. *Chinese Journal of Mechanical Engineering*, 2016, 29(3): 556–563.
31. CHRISTOPHER J, CHOUDHARY B K, ISAAC E S, et al. Tensile flow and work hardening behaviour of 9Cr-1Mo ferritic steel in the frame work of Voce relationship[J]. *Materials Science and Engineering: A*, 2011, 528(21): 6589–6595.
32. MITTRA J, DUBEY J S, KULKAMI U D, et al. Role of dislocation density in raising the stage II work-hardening rate of alloy 625[J]. *Materials Science and Engineering: A*, 2009, 512(1–2): 87–91.
33. KOCKS U F, MECKING H. Physics and phenomenology of strain hardening: the FCC case[J]. *Progress in Materials Science*, 2003, 48(3): 171–273.
34. FEAUGAS X. On the origin of the tensile flow stress in the stainless steel AISI 316L at 300 K: back stress and effective stress[J]. *Acta Materialia*, 1999, 47(13): 3617–3632.
35. DINI G, UEJI R, NAJAFIZADEH A, et al. Flow stress analysis of TWIP steel via the XRD measurement of dislocation density[J]. *Materials Science and Engineering: A*, 2010, 527(10–11): 2759–2763.
36. MOMENI A, DEHGHANI K, EBRAHIMI G R. Modeling the initiation of dynamic recrystallization using a dynamic recovery model[J]. *Journal of Alloys and Compounds*, 2011, 509(39): 9387–9393.
37. MECKING H, KOCKS U F. Kinetics of flow and strain-hardening[J]. *Acta Metall*, 1981, 29(11): 1865–1875.
38. PENG Xiaona, GUO Hongzhen, SHI Zhifeng, et al. Study on the hot deformation behavior of TC4-DT alloy with equiaxed $\alpha + \beta$ starting structure based on processing map[J]. *Materials Science and Engineering: A*, 2014, 605: 80–88.

Fengkuil CUI born in 1957, is currently a professor at *Henan University of Science and Technology, China*. He received his PhD degree from *Xi'an University of Technology, China*, in 2007. His research interest is advanced manufacturing technology. E-mail: cuifk2008@163.com.

Yuanfei LING born in 1990, is currently a PhD candidate at *National and Local Joint Engineering Laboratory of Gas Drainage in Complex Coal Seam, Chongqing University, China*. He received his master degree from *Henan University of Science and Technology, China*, in 2016. His research interests include advanced manufacturing technology and water jet. E-mail: 18937976427@163.com.

Jinxue XUE born in 1965, is currently an associate professor at *Henan University of Science and Technology, China*. He received his PhD degree from *Tongji University, China*, in 2011. His research interest is precision machining of hard and brittle materials.

Jia LIU born in 1992, is currently a master candidate at *Henan University of Science and Technology,* China. Her research interest is ultrasonic vibration machining.

Yuhui LIU born in 1989, is currently a master candidate at *Henan University of Science and Technology,* China. His research interest is advanced manufacturing technology.

Yan LI born in 1960, is currently a professor and vice president of *Xi'an University of Technology, China*. His research interests are unconventional machining technology, deep hole processing and forming technology.